Relation among Potential, Fluctuation Change and L-H Transition in the JFT-2M Tokamak

Y.MIURA 1), T.IDO 2), K.KAMIYA 1), Y.HAMADA 2) and JFT-2M GROUP 1)

1) Japan Atomic Energy Research Institute, Ibaraki, 311-0193, Japan
2) National Institute for Fusion Science, Gifu, 509-5292 Japan

e-mail contact of the main author: miura@naka.jaeri.go.jp

Abstract. Potential and density/temperature fluctuation at L-H transition are measured by the heavy ion beam probe (HIBP) on JFT-2M. It has been observed that the time scale of potential change is as fast as 10-100μs when the input power (P_{in}) is larger than the L-H threshold power (P_{th}). When P_{in}~P_{th}, the confinement is improved gradually step by step with sawteeth crashes accompanied with the decrease of potential. After a few sawteeth crashes, potential drops rapidly to the level of the ELM-free H-mode. From the gradual change of the potential with assuming that dE_r/dr is a key to form and to sustain the transport barrier, the criterion of the dE_r/dr is less than $(1.2 \pm 0.4)\times10^3$ kV/m^2. At an ELM just before H-L transition, the potential inside the separatrix also shows the rapid positive jump. The time scale of the positive jump and its recover to its negative value is about 40μsec and 150μsec, respectively. Before the H-L transition, the time between ELMs and/or dithering transition becomes shorter and the plasma finally goes back to L-mode.

1. Introduction

The important role of radial electric field (E_r) in a tokamak plasma confinement was pointed out [1] in a process to clarify the physical mechanism of H-mode discovered first in ASDEX [2]. It has been shown theoretically [1,3] and experimentally [4,5] that E_r is closely connected to the improved confinement. H.Biglari et al indicated theoretically that a sheared rotation could suppress turbulence which induces anomalous transport [6]. The suppression of the turbulence by **E**x**B** shear is the most credible model recently. The important role of E_r is demonstrated in L-H transition achieved by a biased external electrode [7,8] and the results in TEXTOR support the proposed model [6]. However, the temporal behavior of E_r has never been measured directly with a time resolution enough to test the theoretical predictions [3,9].
Recently, the change of the potential at L-H transition is observed with a high time resolution (~2μs) by a heavy ion beam probe (HIBP [10]) diagnostic in the JFT-2M Tokamak [11,12]. It is shown that the potential changes rapidly at L-H transition triggered by a sawtooth crash. In this paper, we would like to discuss about the time scale of the potential change at L-H and ELM just before H-L transition, and the relation among the potential change, the change of the fluctuation and the transport barrier.

2. Experimental Setup

The HIBP is a diagnostic to measure a local electrostatic potential in high temperature plasmas directly. Singly charged heavy ion beam (Tl^{1+}), called the primary beam, is injected into the magnetically confined plasma (see Fig.1). A part of the primary beam is charged

doubly through the electron impact ionization and it is called the secondary beam (Tl^{2+}). Since the charge number increases from one to two, the total energy of the injected ion changes by the potential energy at the ionization point. The kinetic energy of the secondary beam ion outside of the plasma changes because of total energy conservation (Fig.1 (b)). Therefore, the local potential at the ionization point can be obtained through the measurement of the difference of the kinetic energies between the primary and the secondary beam ion. The primary beam intensity should be set large enough to measure the potential with a high time resolution of about 1μs. The fluctuation of the intensity of the secondary beam reflects the local density fluctuation, although the coupling of the electron density (n_e) and temperature (T_e) fluctuation on the beam trajectory must be take into account. Thus, an HIBP is useful to study the physical mechanism of improved confinement which may relate the reduction of density fluctuation by sheared **E**x**B** flow. We have installed a 500keV HIBP, which was previously used in JIPPT-IIU [13], on the JFT-2M tokamak [14] in order to study the physics of L-H transitions. It can measure the potential with the time resolution of about 2μs.

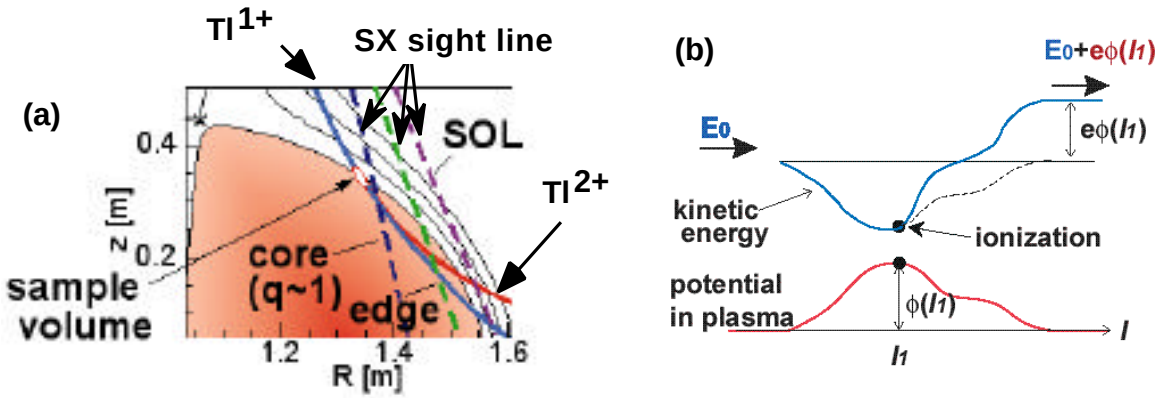

Fig. 1 (a)HIBP diagnostic on JFT-2M. The sample volume is set at the edge to study an L-H transition. The important Soft X-ray (SX) sight lines are also shown. (b)The principle of potential measurement. The horizontal axis is the distance along the beam trajectory and l_1 indicates the position of ionization of the primary beam (Tl^{1+}). The secondary beam ion (Tl^{2+}) gains the potential energy of $e\phi(l_1)$ due to the ionization.

2. Time Scale of the Potential Change

Figure 2 (a)-(c) show the temporal behaviors of the potential change near the separatrix and Soft X-ray (SX) intensity at L-H transition in the case of $P_{NBI}>P_{th}$. In this case, the beam of HIBP was fixed to measure the potential change with the fastest time resolution. In the case of Fig.2 (a), the change of the very rapid drop of the potential is observed with the drop of the fluctuation [11]. The time scale of its change is 12μs in this shot. However, it is not a typical behavior even with the same experimental condition. There is a variation and shows the two step of the potential drop in the most of the L-H transition as shown in Fig.2 (b) and (c). It shows that the potential drops after the sawtooth with its time scale of about 100μs or

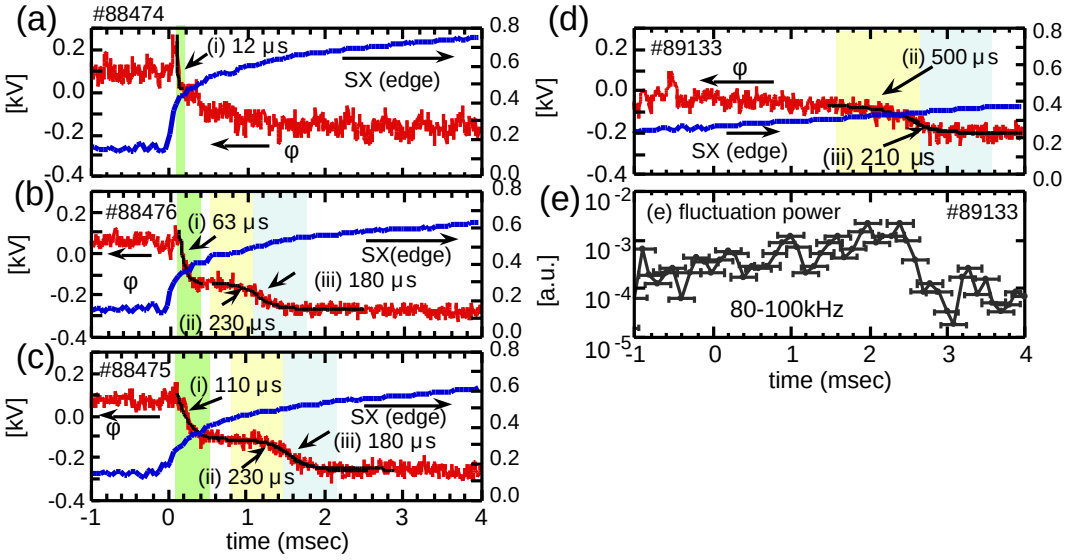

Fig. 2 Temporal behaviors of the potential change near the separatrix and edge SX intensity. From (a) to (c) show the case of $P_{NBI}>P_{th}$ and (d) shows the case of $P_{NBI}\sim P_{th}$. The times shown in the figures are the characteristic time by the exponential fitting for the potential drop. (e) The temporal behavior of the fluctuation power in the case of $P_{NBI}\sim P_{th}$ (the same shot for (d)). The time of zero in the horizontal axis means the time of the arrival of the heat pulse at the edge.

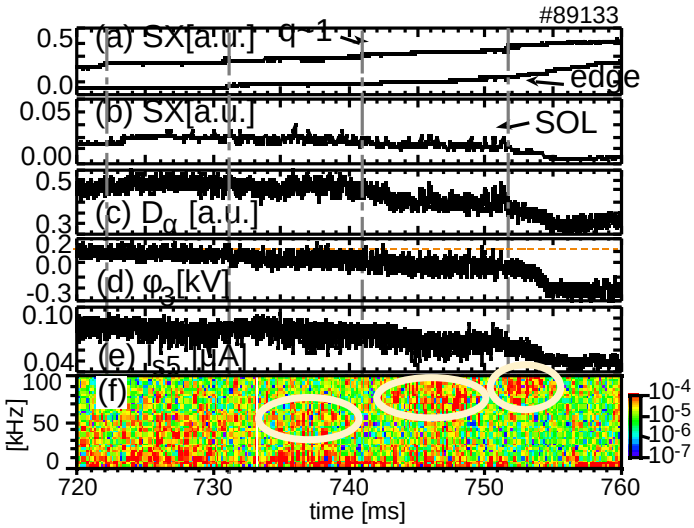

Fig. 3 Temporal behaviors of potential and density/temperature fluctuation at L-H transition. (a) SX intensities from core and edge, (b)SX intensity from SOL, (c) D_α intensity, (d) Potential (ds=-0.4 cm). The dotted line indicates the L-mode level. (e) Secondary beam intensity (ds=+0.1 cm), (f) Power of the fluctuation of secondary beam intensity of (e). The vertical lines indicate the time of sawteeth crashes. The ds is the distance from separatrix and positive (negative) value means outside (inside) separatrix.

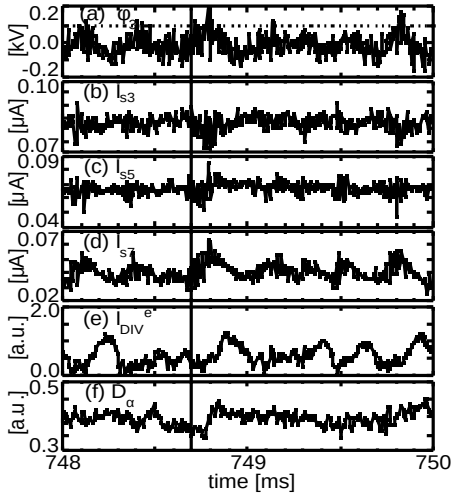

Fig. 4 The typical bursting phenomenon after the start of the formation of the transport barrier. The shot is the same as Fig.3. (a) Potential (ds=-0.4 cm). (b), (c), and (d) show secondary beam intensities at ds=-0.4, +0.1, and +0.6 cm, respectively. (e) Electron saturation current on the divertor plate. (f) D_α intensity

less. It is the order of the transit time of collisionless banana ion (~50μs for 300eV, D^+). The potential stays constant for about one millisecond after that, and drops again with the time scale of a few hundreds microsecond accompanied with the suppression of the high frequency fluctuation (Fig.2 (e) shows the case of $P_{NBI}\sim P_{th}$, but the behavior is the same). Figure 3 shows the temporal history of SX and D_α intensities, potential, the secondary beam

intensity and the frequency spectrum of the fluctuation of the secondary beam intensity at L-H transition in the case of P_{NBI}~P_{th}. The heating stars form 700msec and the period of sawteeth increases and saturates in about 10ms. The L-H transition is not clearly triggered by one sawtooth crash in this case. By the sawtooth crash at 731ms, potential, D_α intensity and SX intensity from SOL show a little drop, and they show further drop by the next crash at 740.9ms. They show the final drop at about 2ms after the sawteeth crash at 751.8ms without any event such as sawtooth. These drops indicate the formation of the transport barrier at the edge step by step with sawtooth crash. Figure 3 (f) shows the image plot of the frequency spectrum of the fluctuation. The spectrum separates in two components after the sawtooth crash at 731ms. One is the fluctuation with the frequency of 10kHz or less and the other is the fluctuation with the higher frequency. The frequency of the latter increases step by step with sawtooth crash [50kHz (around 737ms) → 80kHz (around 747ms) → 100kHz (around 751ms)]. The increase of the frequency may reflect the Doppler shift due to the increase of the **E**x**B** rotation of the plasma. After the start of the formation of the barrier at 731ms, the fluctuation of a bursting character appears in the potential and the secondary beam intensity of the HIBP. Its repetition frequency is 2-4kHz and decreases gradually. It corresponds to the lower frequency component in Fig.3 (f). The potential jumps to the L-mode level shown by the dashed line at onset of the burst (see Fig.3 (d)). The typical bursting phenomena in the potential, the secondary beam intensity, the electron saturation current on the divertor plate (I_{DIV}^e), and D_α intensity are shown in Fig.4. Let's see the time at around 748.7ms (vertical line in Fig.4). When the positive jump of the potential signal (Fig.4 (a)) is observed, the secondary beam intensity from the inside separatrix (Fig.4 (b)) decreases, that from the outside separatrix (Fig.4 (d)) increases, and the intensity of I_{s5} is a pivot at the onset of the burst. It means that the density and/or temperature inside separatrix decrease and those outside separatrix increase. The I_{DIV}^e also increases with the delay of about 100μs. They indicate the intermittent increase of the radial heat and particle flux caused by the burst. The burst may reflect the repetition of the formation and collapse of the transport barrier. Coming back to Fig.1 (d), it shows the temporal behavior of the potential change in the case of P_{NBI}~P_{th}. Since the potential drops step by step with the sawtooth crash, there is no rapid potential drop at t=0, but the second drop of the potential as observed in the case of P_{NBI}>P_{th} is observed with the suppression of the high frequency fluctuation (Fig.1 (e)). Since the time scale of the change shows the similar value of the second potential drop as observed in the case of P_{NBI}>P_{th}, we think that the drop of the potential with the time scale of a few hundreds microsecond is caused by a similar mechanism.

3. Potential Change at ELM just before H-L transition

Since the duration of the data acquisition system of HIBP is limited, H-L transition was studied by reducing the heating duration of 66msec. In this case, H-mode is sustained about 50msec after switching off the heating neutral beam. It is a few times longer than the slowing down time of 32keV-hydrogen beam. The termination of H-mode occurs by ELM and/or dithering transition. Figure 5 shows the first and second ELMs which occur ~38msec after switching off the beam. The potential inside the separatrix shows the rapid positive

jump at ELM (Fig.5 (b)). The time scale of the jump is about 40μsec. The intensity of the secondary beam drops at ELM and recovers about 1.5msec after the ELM. It means that the density and/or temperature recover about the time scale of 1.5msec. The recover of the potential of its negative value is rapid. The time scale of the drop is about 150μsec. Comparing with the L-H transition, the time scale is different from that of the first or second drop of the potential. Moreover, the two step drop of the potential is not observed in this case. The fluctuation power of the secondary beam intensity shows that the high frequency fluctuation (50-150kHz) increases before the ELM and it disappears when the potential is dropping. These behaviors are similar to the first drop of the potential at L-H transition with suppressing the high frequency fluctuation. The high frequency fluctuation before the ELM tends to increase after switching off the beam (reducing the heating power). Since the poloidal rotation is kept almost constant during H-phase (even after switching off the beam), then it does not depends on the poloidal rotation velocity. After the ELMs, the time between ELMs becomes shorter and the duration of L-phase becomes longer. And the plasma finally goes back to L-mode at 715msec (~10msec after the first ELM).

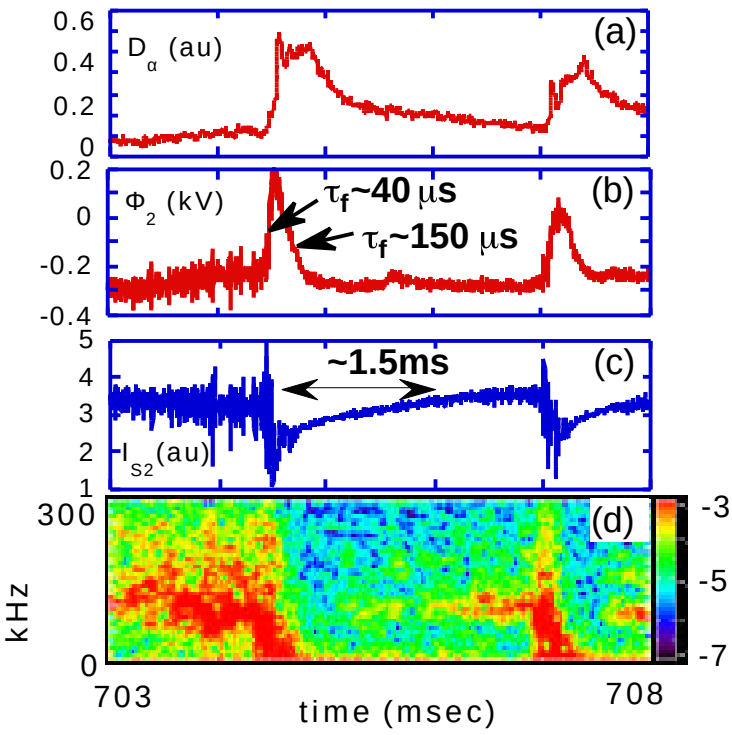

Fig.5 Temporal behaviors at ELM before H-L transition. (a)D_α intensity, (b)Potential (ds=-0.3cm). (c)Secondary beam intensity (ds=-0.3 cm) (d)Power of the fluctuation of secondary beam intensity of (c).

4. Relation between Electric Field Structure and Transport Barrier Formation

Figure 6 (b) shows the measured potential profiles. The each time of the potential profiles corresponds to the hatched periods in the time trace of D_α intensity of Fig.6 (a). The E_r and the gradient of E_r (dE_r/dr) are shown in Fig.6 (c) and (d), respectively. This is the case of P_{NBI}~P_{th}, therefore the plasma goes to H-mode step by step with the sawtooth crash from 737msec. Since there is a little ambiguity in the estimation of the position of the sample volume, the possible position of the separatrix (ds=0) is in the region labeled "separatrix" in the figure. The E_r and dE_r/dr are estimated by fitting a function of **tanh** to the measured potential profiles. The profile of both E_r and dE_r/dr around the separatrix in the L-mode phase [A] is flat and there is almost no shear of the radial electric field. The profiles of [C]

and [E] are the time of ELM-free H-mode and show very similar shape. The peak value of dE_r/dr reaches about 4000kV/m^2. In the beginning phase of the transport barrier formation (hatched period [B]), the peak of dE_r/dr exceeds $(1.2\pm0.4)\times10^3$ kV/m^2. Assuming that dE_r/dr is a key to form and to sustain the transport barrier, the criterion is less than $(1.2\pm0.4)\times10^3$ kV/m^2. In the profile of [D], it clearly shows that the width of the large dE_r/dr becomes narrower. In this period from 765msec to 785msec, the increase of D_α intensity can be clearly observed and the decrease of time derivative of stored energy, dW_{MHD}/dt, is observed (about 40% reduction). And the dW_{MHD}/dt recovers form 785msec. The time period like this state is called H'-mode and the coherent mode of the density fluctuation [15] is observed like EDA in the ALCATOR-CMOD[16]. Figure 7 shows that the contour plot of SX intensity measured by the PIN diode array. The lines of sight are shown in Fig.7 (b). The gradient of the SX intensity at edge increases during the time period from 765msec to 785msec, but there is a flat area just inside of the steep gradient. It means that the pedestal width decrease in this period. The special resolution of the SX measurement is not enough to compare with the width of dE_r/dr quantitatively. We think the degradation of the

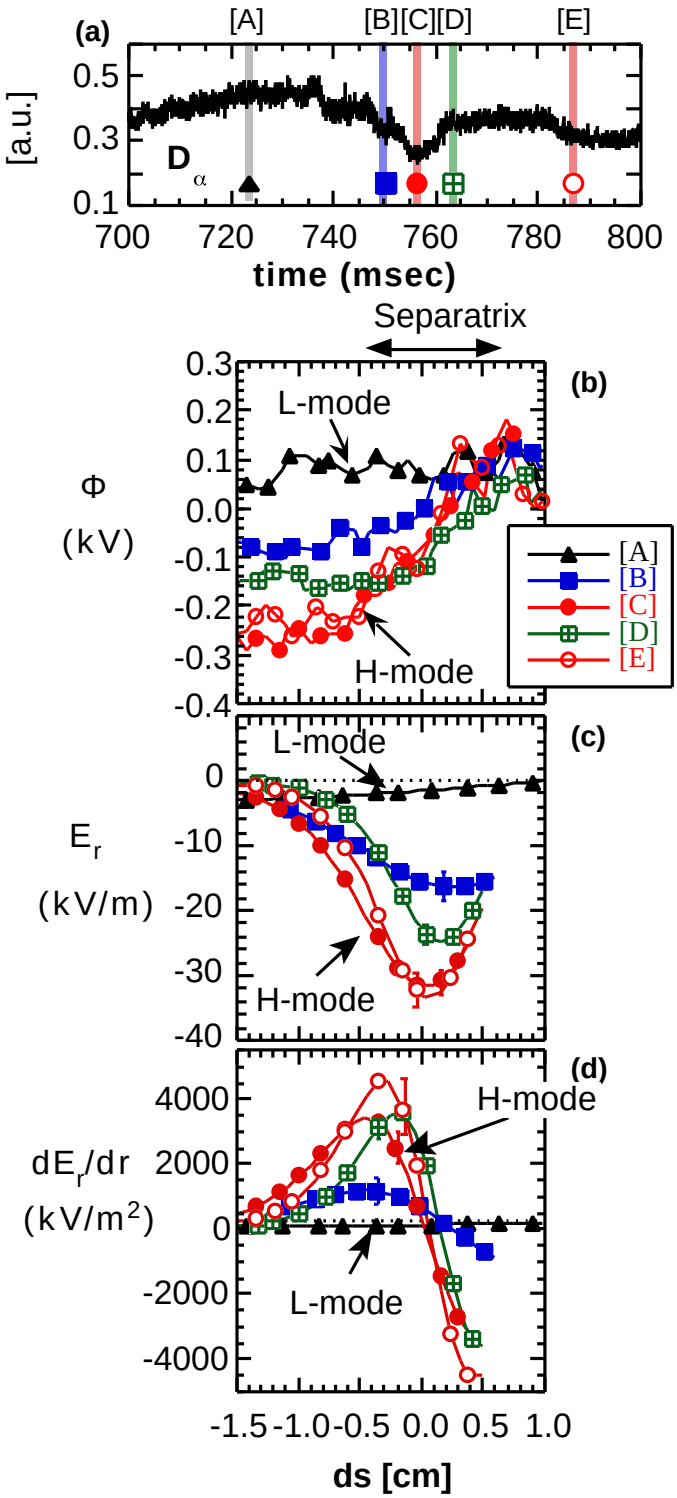

*Fig. 6 (a)The temporal behaviors of the D_α intensities in the case of $P_{NBI}\sim P_{th}$. (b)The measured potential profile by sweeping the primary beam with the sweep rate of 0.17mm/μs and with the repetition frequency of 600Hz. The hatched periods in (a) show the measured time. (c) and (d) show E_r and dE_r/dr, respectively. These are estimated by fitting a function of **tanh** to the measured potential profile.*

confinement of H'-mode is due to the reduction of the pedestal width that might have a strong relation with the width of large dE_r/dr.

5. Discussion and Summary

The change of the radial electric filed shown in Ref.[17] is as follows,

$$\varepsilon_0\varepsilon\ \Delta E_r / \Delta t = e\left(\Gamma_{e-i}^{anom} - \Gamma_i^{lc} - \quad\right).$$

The first term in the right hand side, $\Gamma_{e\text{-}i}^{anom}$, is the contribution of the bipolar part of the anomalous cross-field flux. The second one, Γ_i^{lc}, is the flux by the loss cone loss of ions. And there are many processes such as the flux by the Reynolds stress and etc. The clarification of the Δt makes it possible to find a physical mechanism of L-H transition. Since the time scale of the potential change just after a sawtooth (10-100μs) is the order of the transit time of collisionless banana ion and there is evidence that the flux of collisionless ion shows the rapid change at L-H transition [18], then Γ_i^{lc} might have a large contribution to form the radial electric field. However, the second drop of the potential is not understood yet.

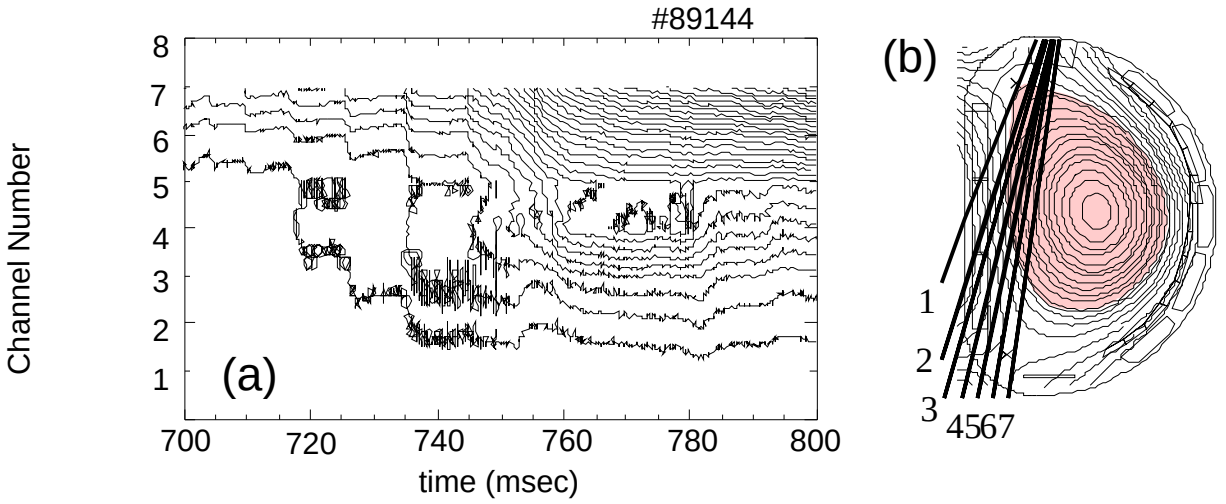

Fig. 7 (a)Contour plot of the SX intensity for the shot shown in Fig.6. (b) shows the line of sight of the SX measurement. In the period from ~765msec to ~785msec, it is called H'-mode [see Fig.6 (a)].

In summarizing present results, we found that the potential at the edge of the plasma shows the very rapid change at L-H transition and there is a second drop of the potential. The time scale of the former drop is less than 100μsec and that of the latter one is more than 200μsec. Since there is evidence that the flux of collisionless ion shows the rapid change by a sawtooth heat pulse, the collision less ion loss might be attribute to the former drop of the potential. At an ELM, the potential inside the separatrix also shows the rapid positive jump. The time scale of the jump is about 40μsec. The recover of the potential to its negative value is rapid and the time scale of the drop is about 150μsec. Before the H-L transition, the time between

ELMs and/or dithering transition becomes shorter and the duration of L-phase becomes longer. And the plasma finally goes back to L-mode. In the case of $P_{NBI} \sim P_{th}$, the potential, SOL SX, and D_α intensities do not drop clearly just after a sawtooth crash and decrease gradually step by step with sawteeth crashes. In this study with assuming that dE_r/dr is a key to form and to sustain the transport barrier, the criterion of the dE_r/dr is less than $(1.2 \pm 0.4) \times 10^3$ kV/m^2. In the phase of H'-mode after L-H transition, the width of large dE_r/dr becomes narrower. This result might relate to make the pedestal width narrow and to degrade the confinement.

Acknowledgement

We are grateful to Prof.K.Itoh, Prof.S.-I.Itoh, Dr.K.Ida and Dr.T.Takizuka for fruitful discussions and Dr.A.Funahashi, Dr.H.Ninomiya, Dr.M.Azumi, Prof.M.Fujiwara, and Prof.A.Iiyoshi for the continuous encouragement. We would also like to thank Mr.A.Nishizawa for the installation and calibration of the HIBP system. We would also like to thank Prof.J.D.Callen for valuable comments.

References

[1] S.-I. Itoh and K. Itoh, Phys. Rev. Lett. **22** (1988) 2276.
[2] F. Wagner et al., Phys. Rev. Lett. **49** (1982) 1408.
[3] K. C. Shaing and E. C. Crume, Jr., Phys. Rev. Lett., **63** (1989) 2369.
[4] R. J. Groebner, K. H. Burrell and R. P. Seraydarian, Phys. Rev. Lett., **64** (1990) 3105.
[5] K. Ida et al., Phys. Rev. Lett., **65** (1990) 1364.
[6] H. Biglari, P. H. Diamond and P. W. Terry, Phys. Fluids **B 2** (1990) 1.
[7] R. J. Taylor et al., Phys. Rev. Lett., 63 (1989) 2365.
[8] R. R. Weynants, S. Jachmich and G. Van Oostt, Plasma Phys. Control. Fusion, **40** (1998) 635.
[9] K. Itoh, and S.-I. Itoh, Nucl. Fusion, **29** (1989) 1031.
[10] R. L. Hickok, Rev. Sci. Instrum, **38** (1967) 142.
[11] Y. Hamada, et al., 17th IAEA Fusion Energy Conference, IAEA-F1-CN-69/PD (1998).
[12] T. Ido, K.Kamiya, Y. Miura, et al., Plasma Phys. Control. Fusion, **42** (2000) A309.
[13] Y. Hamada, et al., Plasma Phys. Control. Fusion, **36** (1994) 1743.
[14] T. Ido et al., Rev. Sci. Instrum, **70** part II (1999) 955.
[15] K. Shinohara, Y. Miura and K. Hoshino, Journal of Plasma Fusion Research **74** (1998) 607.
[16] M. Greenwald, R. Booivin, P. Bonoli, et al., Plasma Phys. Control. Fusion, **42** (2000) A263.
[17] K. Itoh, Plasma Phys. Control. Fusion **36** (1994) A307.
[18] Y. Miura and JFT-2M Group, Nucl. Fusion **37** (1997) 175.